Supporting Information for

X-ray Emission Spectroscopy at XFEL: Limits to Observation of the Classical Spectroscopic Response for Electronic Structure Analysis

*Scott C Jensen[a], Brendan Sullivan[a,†], Daniel Hartzler[a,‡], Jose Meza Aguilar[b], Salah Awel[c,d], Saša Bajt[e], Shibom Basu[f], Richard Bean[g], Henry Chapman[c], Chelsie Conrad[h], Matthias Frank[i], Raimund Fromme[b], Jose M Martin-Garcia[b], Thomas D Grant[j,k], Michael Heymann[c,l], Mark S. Hunter[m], Gihan Ketawala[h], Richard A Kirian[n], Juraj Knoska[c], Christopher Kupitz[o], Xuanxuan Li[p], Mengning Liang[m], Stella Lisova[n], Valerio Mariani[c], Victoria Mazalova[c], Marc Messerschmidt[k], Michael Moran[b], Garrett Nelson[n], Dominik Oberthür[c], Alex Schaffer[q], Raymond G Sierra[m], Natalie Vaughn[h], Uwe Weierstall[b,n], Max O. Wiedorn[c,], Lourdu Xavier[c,m,§], Jay-How Yang[b], Oleksandr Yefanov[c], Nadia A Zatsepin[n], Andrew Aquila[m], Petra Fromme[b,r], Sébastien Boutet[m], Gerald T Seidler[s], and Yulia Pushkar[a]**

[a]Department of Physics and Astronomy, Purdue University, West Lafayette, IN 47907, USA

[b]Biodesign Institute, Arizona State University, Tempe, AZ 85287-7401, USA

[c]Center for Free-Electron Laser Science, Deutsches Elektronen-Synchrotron, D-22607 Hamburg, Germany

[d]The Hamburg Center for Ultrafast Imaging, Universität Hamburg, 22761 Hamburg, Germany

[e]Photon Science, Deutsches Elektronen-Synchrotron, D-22607 Hamburg, Germany

[f]Paul Sherrer Institut, 5232 Villigen PSI, Switzerland

[g]European XFEL GmbH, Hamburg, D-22671, Germany

[h]Department of Chemistry and Biochemistry, Arizona State University, Tempe, AZ 85287-7401, USA

[i]Lawrence Livermore National Laboratory, Livermore, CA 94550, USA

[j]Hauptman-Woodward Institute, Department of Structural Biology, Jacobs School of Medicine and Biomedical Sciences, SUNY University at Buffalo, Buffalo, NY 14203

[k]BioXFEL Science and Technology Center, Buffalo, NY 14203, USA

[l]Max Planck Institute of Biochemistry, 82152 Planegg, Germany

[m]SLAC National Accelerator Laboratory, Menlo Park, California 94025, USA

[n]Department of Physics, Arizona State University, Tempe, AZ 85287-7401, USA
[o]Department of Physics, University of Wisconsin-Milwaukee, Milwaukee, WI 53201, USA
[p]Beijing Computational Science Research Center, Beijing 100193, China
[q]Department of Biochemistry, University of California Davis, Davis, CA 95616, USA
[r]School of Molecular Sciences, Arizona State University, Tempe, AZ85287-1604
[s]Department of Physics, University of Washington, Seattle, Washington 98195-1560, USA

Corresponding Author

* Corresponding author ypushkar@purdue.edu

Current Affiliation

[†]Neutron Scattering Division, Oak Ridge National Laboratory, Oak Ridge, TN 37830, USA

[‡]AECOM, 626 Cochrans Mill Road, Pittsburgh, PA 15263, USA

[§]Max-Planck Institute for the Structure and Dynamics of Matter, D-22761 Hamburg, Germany

Methods and Procedures

Beamline Parameters

The experiment was performed at the Coherent X-ray Imaging instrument[1] at the Linac Coherent Light Source (Menlo Park, USA) XFEL[2]. In order to achieve high X-ray flux density, the incoming X-ray beam was focused by a set of Kirkpatrick-Baez mirrors which typically results in a spot size of 1.3 μm (FWHM) which is used here, however values for the FWHM could range up to 2.3 μm. An upstream gas monitor measured the pulse energy and was read out each shot. The number of photons was estimated from the pulse energy and assuming an estimated 60% X-ray transmission efficiency through the X-ray optics to the downstream interaction point.

Data were taken over two beamtimes (LJ49 and LL23), one at the incident photon energy of 6.9 keV with a pulse duration of 20 fs and 40 fs and the second at 8.7 keV with 16 fs and 34 fs pulse duration. The experiment was monitored in real time using the OnDA software package[3]. In the second beamtime the time structure of the micro-bunched electrons was also recorded on a pulse by pulse basis using the X-band radio-frequency deflector[4]. Background images were taken approximately every two hours to ensure proper calibration. This information was used to sort data by pulse duration more precisely.

Sample Preparation and Delivery

The sample was prepared by dissolving $MnCl_2 \bullet (H_2O)_4$ from Sigma Aldrich in a solution of ethanol except one dataset (40 fs at 6.9keV) taken with water, all had a final concentration of 1 Molar. Both gas-dynamic virtual nozzles[5] and double flow focusing nozzles[6] were used to deliver the $MnCl_2$ in an ~5 μm diameter jet into the interaction region. The difference between these two delivery types, as the name suggests, is the medium around the sample that ensures the ejected medium maintains a constant stream. A jet flow rate of ~5-40 μl/min was used with a 40μm diameter exit port in the nozzle. The jet diameter varied with throughout the run with an estimated ~5μm-20μm in diameter. Fresh sample was delivered for every X-ray pulse and X-ray source was operating at 120 Hz. Discarded sample was collected using a small aluminum catcher inside of the vacuum chamber directly below the interaction region.

Powder Mn oxides were measured using X-ray pulses with 100 μm FWHM spot size at a few points during the second beamtime(LL23). This was done by inserting a sample holder at the interaction region with the oxides sealed in Kapton tape. No spectral changes were found between X-ray exposures on the same sample.

X-ray Emission Detection

A von Hamos X-ray emission spectrometer[7] was used to spatially resolve both the manganese $K\beta_{1,3}$ and $K\beta'$ emission lines. The 6.9 keV data (beamtime #1) were recorded using a CSPAD[8] and the 8.7 keV data were recoded using the newly commissioned ePix [9] area detectors. Both detectors have gaps in the detection surfaces between modules which appears between 6499.8-6500.3 eV emission energies for data collected with 20 fs pulses at 6.9 keV, 6490.1-6490.6 eV for data collected with 40 fs pulses at 6.9 keV and between 6483-6484 eV for all data sets obtained using 8.7 keV incident energy. Spectral intensities for missing pixels were obtained by linear interpolation between the two nearest data points.

Due to internal space constrains of the set up, the von Hamos spectrometer was tilted ~15 degrees from the vertical to record maximal accessible spectral range. In the second beamtime, LL23, (8.7 keV incident energy) due to additional setup optimizations a larger energy range was recorded which included the $K\beta'$ emission line unlike those reported previously.[10]

Spectra recorded at an angle were analyzed using a bilinear interpolation[11]. This interpolation method was used by taking evenly spaced steps along the dispersion direction and weighting the surrounding pixel distances and intensities to assign a value to the new point. The resultant energy spectra were calibrated using the known theoretical energy vs distance function from the analyzers and one or two points from standards, including $MnCl_2$ sample collected at a low X-ray beam intensity.

Rate Equation Model

The rate equations were based on cross sections and excited state lifetimes calculated by XATOM, the photon flux density and pulse duration. A system of equations was created by considering the absorption of X-rays that ionize 1s electrons and the decay pathways that fill the 1s hole, see Figure 3A. A symbolic rate equation with i, the number of current 1s holes, and j, the total number of ionization events, can be written as

$$\frac{dS_j^i}{dt} = A^{i-1}S_{j-1}^{i-1} + D_j^{i+1}S_j^{i+1} - A^iS_j^i + D_j^iS_j^i$$

Where A is the absorption rate and D is the decay rate of the indicated state.

The system of linear differential equations obtained from this system was solved symbolically using Maple 2017. Here we account for the beam's Gaussian profile by solving the system of equations for radial sections of an uncorrelated (p=0) bivariate Gaussian (30 sections of equal radial steps ranging from 0 to three times the FWHM). The solution of each term was normalized using the percent of X-rays in that step range, thereby accounting for highly exposed areas yielding more to the fluorescent signal.

The average number of electron holes per 1s ionization was estimated to be equivalent to the holes in S_1^0 state after all 2s and 2p holes, lifetimes of 0.2-2 fs, are filled through additional decays as calculated using XATOM. This fundamental model also used the following assumptions: 1) X-ray intensity doesn't change with sample thickness (<10% absorption for all samples used here), 2) absorption events caused by orbitals other than the 1s were ignored (~10% contribution in our experiments), and 3) near identical values for decay rates were found using XATOM for states representing multiple electronic configurations, which led to the use of a single decay value for each state shown in Figure 3A.

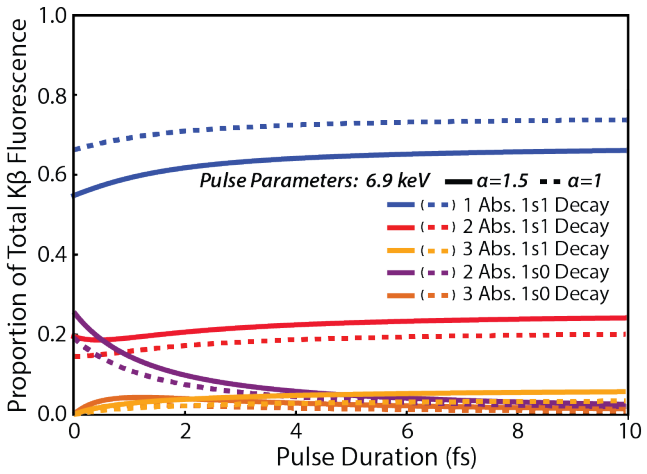

SI Figure 1. Emission from different states shown in main text Figure 2A as a function of pulse duration. Percentages of emissions by source is normailized including the 1s0 states whose emission is unlikely to overlap those of the 1s1 emission.

SI Table 1. Parameters shown for X-ray emission data taken from MnCl2 in solution for our data compared to two previous works.

	Pulse Duration	Photon Energy	α
Presented work	20 fs	6.9 keV	0.015 – 1.4
	40 fs	6.9 keV	0.026 – 2.2
	16 fs	8.7 keV	0.0037 – 0.70
	34 fs	8.7 keV	0.013 – 0.77
Low Dose [10]	50 fs	7 keV	0.49
	100 fs	7 keV	0.15
	50 fs	9.5 keV	0.25
	100 fs	9.5 keV	0.08
Stimulated Emission[12]	10 fs	6.6 keV	2.4 - 18
	30 fs	6.6 keV	2.4 - 18

SI Table 2 and 3. Photoelectric cross section by orbital for Mn^{2+} (Table 1) and with a single 1s hole (Table 2) for 6.9keV.

Orbital	Cross Section (um^2)	Percent of total cross section
1s	3.18×10^{-12}	88.12%
2s	2.21×10^{-13}	6.12%
2p	1.57×10^{-13}	4.34%
3s	3.13×10^{-14}	0.87%
3p	1.96×10^{-14}	0.54%
3d	2.87×10^{-16}	0.01%
Total	$3.61E \times 10^{-12}$	

Orbital	Cross Section (Mb)	Percent of total cross section
1s	1.65×10^{-12}	77.49%
2s	2.38×10^{-13}	11.14%
2p	1.83×10^{-13}	8.60%
3s	3.47×10^{-14}	1.63%
3p	2.38×10^{-14}	1.12%
3d	4.68×10^{-16}	0.02%
Total	2.13×10^{-12}	

SI Table 4. Decay pathways and yields are shown for a 1s hole in Mn^{2+}. Lifetimes were calculated using the XATOM software. The first major relaxation pathways are highlighted for reference.

	Decay pathway	Percent Yield	Unfilled shells	Lifetime (fs)
Fluorescence	1s - 2p	30.10%	2p5	1.7
	1s - 3p	3.70%	3p5	29000.0
Auger	1s - 2s 2s	3.90%	2s0	0.12
	1s - 2s 2p	13.40%	2s1 2p5	0.24
	1s - 2s 3s	1.00%	2s1 3s1	0.23
	1s - 2s 3p	1.70%	2s1 3p5	0.23
	1s - 2s 3d	0.00%	2s1 3d4	0.28
	1s - 2p 2p	35.50%	2p4	0.72
	1s - 2p 3s	1.60%	2p5 3s1	1.4
	1s - 2p 3p	8.00%	2p5 3p5	2
	1s - 2p 3d	0.30%	2p5 3d4	1.8
	1s - 3s 3s	0.10%	3s0	5
	1s - 3s 3p	0.20%	3s1 3p5	10
	1s - 3s 3d	0.00%	3s1 3d4	16.7
	1s - 3p 3p	0.40%	3p4	15000.0
	1s - 3p 3d	0.00%	3p5 3d4	38000.0
	1s - 3d 3d	0.00%	3d3	Na

1. Liang, M. N.; Williams, G. J.; Messerschmidt, M.; Seibert, M. M.; Montanez, P. A.; Hayes, M.; Milathianaki, D.; Aquila, A.; Hunter, M. S.; Koglin, J. E., et al. The Coherent X-ray Imaging instrument at the Linac Coherent Light Source. *J. Synchrotron Radiat.* **2015,** *22*, 514-519.
2. Emma, P.; Akre, R.; Arthur, J.; Bionta, R.; Bostedt, C.; Bozek, J.; Brachmann, A.; Bucksbaum, P.; Coffee, R.; Decker, F. J., et al. First lasing and operation of an angstrom-wavelength free-electron laser. *Nat. Photon.* **2010,** *4* (9), 641-647.
3. Mariani, V.; Morgan, A.; Yoon, C. H.; Lane, T. J.; White, T. A.; O'Grady, C.; Kuhn, M.; Aplin, S.; Koglin, J.; Barty, A., et al. OnDA: online data analysis and feedback for serial X-ray imaging. *J. Appl. Crystallogr.* **2016,** *49* (3), 1073-1080.
4. Ratner, D.; Behrens, C.; Ding, Y.; Huang, Z.; Marinelli, A.; Maxwell, T.; Zhou, F. Time-resolved imaging of the microbunching instability and energy spread at the Linac Coherent Light Source. *Phys. Rev. ST Accel. Beams.* **2015,** *18* (3).
5. DePonte, D. P.; Weierstall, U.; Schmidt, K.; Warner, J.; Starodub, D.; Spence, J. C. H.; Doak, R. B. Gas dynamic virtual nozzle for generation of microscopic droplet streams. *J. Phys. D: Appl. Phys.* **2008,** *41* (19).
6. Oberthuer, D.; Knoska, J.; Wiedorn, M. O.; Beyerlein, K. R.; Bushnell, D. A.; Kovaleva, E. G.; Heymann, M.; Gumprecht, L.; Kirian, R. A.; Barty, A., et al. Double-flow focused liquid injector for efficient serial femtosecond crystallography. *Sci. Rep.* **2017,** *7*.
7. Alonso-Mori, R.; Kern, J.; Sokaras, D.; Weng, T.-C.; Nordlund, D.; Tran, R.; Montanez, P.; Delor, J.; Yachandra, V. K.; Yano, J., et al. A multi-crystal wavelength dispersive x-ray spectrometer. *Rev. Sci. Instrum.* **2012,** *83* (7), 073114-073114.
8. Hart, P.; Boutet, S.; Carini, G.; Dubrovin, M.; Duda, B.; Fritz, D.; Haller, G.; Herbst, R.; Herrmann, S.; Kenney, C., et al. The CSPAD megapixel x-ray camera at LCLS. *Proc. SPIE* **2012,** *8504*, 85040C.
9. Blaj, G.; Caragiulo, P.; Carini, G.; Dragone, A.; Haller, G.; Hart, P.; Hasi, J.; Herbst, R.; Kenney, C.; Markovic, B., et al. Future of ePix detectors for high repetition rate FELs. *AIP Conf. Proc. Appl. Phys. Lett* **2016,** *1741* (334), 40012-40099.
10. Alonso-Mori, R.; Kern, J.; Gildea, R. J.; Sokaras, D.; Weng, T.-C.; Lassalle-Kaiser, B.; Tran, R.; Hattne, J.; Laksmono, H.; Hellmich, J., et al. Energy-dispersive X-ray emission spectroscopy using an X-ray free-electron laser in a shot-by-shot mode. *Proc. Natl. Acad. Sci. U.S.A.* **2012,** *109* (47), 19103-19107.
11. Glasbey, C. A.; Mardia, K. V. A review of image-warping methods. *J. Appl. Statist.* **1998,** *25* (2), 155-171.
12. Kroll, T.; Weninger, C.; Alonso-Mori, R.; Sokaras, D.; Zhu, D.; Mercadier, L.; Majety, V.; Marinelli, A.; Lutman, A.; Guetg, M., et al. Stimulated X-Ray Emission Spectroscopy in Transition Metal Complexes. *Phys. Rev. Lett.* **2018,** *120* (13), 133203.